

Article

On the Application of K-User MIMO for 6G Enhanced Mobile Broadband [†]

Anil Kumar Yerrapragada *  and Brian Kelley

Department of Electrical and Computer Engineering, University of Texas at San Antonio, San Antonio, TX 78249, USA; dr.brian.kelley@gmail.com

* Correspondence: anilkumar.yerrapragada@utsa.edu

[†] This paper is an extended version of our paper published in: Yerrapragada, A.K.; Kelley, B. Very High Throughput Internet of Things Networks with K Access Points and K Devices. In proceedings of the MILCOM 2019—2019 IEEE Military Communications Conference (MILCOM), Norfolk, VA, USA, 12–14 November 2019.

Received: 4 October 2020; Accepted: 1 November 2020; Published: 2 November 2020



Abstract: This paper presents a high-throughput wireless access framework for future 6G networks. This framework, known as K-User MIMO, facilitates all-to-all communication between K access points and K mobile devices. For such a network, we illustrate the demodulation of K^2 independent data streams through a new interference cancellation beamforming algorithm that improves spectral efficiency compared to massive MIMO. The paper derives a multi-user Shannon Capacity formula for K-User MIMO when K is greater than or equal to 3. We define an Orthogonal Frequency Division Multiplexing (OFDM) frame structure that demonstrates the allocation of time-frequency resources to pilot signals for channel estimation. The capacity formula is then refined to include realistic pilot overheads. We determine a practical upper-bound for MIMO array sizes that balances estimation overhead and throughput. Lastly, simulation results show the practical capacity in small cell geometries under Rayleigh Fading conditions, with both perfect and realistic channel estimation.

Keywords: beyond-5G; 6G; MIMO; interference alignment; K-User MIMO; OFDM

1. Introduction

The goal of 5G is to enable a fully connected society such that instant information is available just a touch away. 5G achieves this through three key paradigms viz., enhanced Mobile Broadband (eMBB) for gigabit data rates, Ultra Reliable and Low Latency Communications (URLLC) for latency less than 1ms, and massive Machine-Type Communications (mMTC) for 1 million connected devices/sq. km [1,2]. These paradigms are supported by a multilayer technology strategy including small cell architectures [3,4], millimeter wave communication, and massive MIMO. Millimeter wave systems facilitate communication in the high Radio Frequency (RF) bands using analog, digital, and hybrid beamforming [5,6]. Massive MIMO deploys large antenna arrays at base stations and operates in the low to mid RF bands [7–10]. To support the ubiquitous deployment of densely connected networks, this paper investigates an alternative MIMO technology, in the microwave realm, for beyond-5G or 6G networks. This technology, known as K-User MIMO, has the potential to achieve very high throughput compared to 5G Massive MIMO.

Background and Prior Research on K-User MIMO

K-User MIMO is an architecture in which there are K access points and K mobile devices, each equipped with multiple antennas, i.e., spatial dimensions. In the simplest form of K-User MIMO, each Access Point connects to one of the K mobile devices. In this paper, we consider a different form of

K -User MIMO, known as K -User MIMO X, in which each of the K mobile devices receives signals from K access points. This is shown in Figure 1. The all-to-all architecture achieves very high throughput whilst supporting flexibility in achieving diversity. Each of the K access points could send redundant information streams to maximize reliability. Alternatively, they could send unique information streams in order to maximize capacity. K -User MIMO X can switch between these two modes without any change in the mathematics of the algorithm. Further scenarios can be envisioned in which K -User MIMO X allows for adaptive allocation of power to users with more favorable Signal-to-Noise Ratios. Additional encoding of data across time and frequency could be applied so the signals could adapt to malicious behavior such as jamming and eavesdropping.

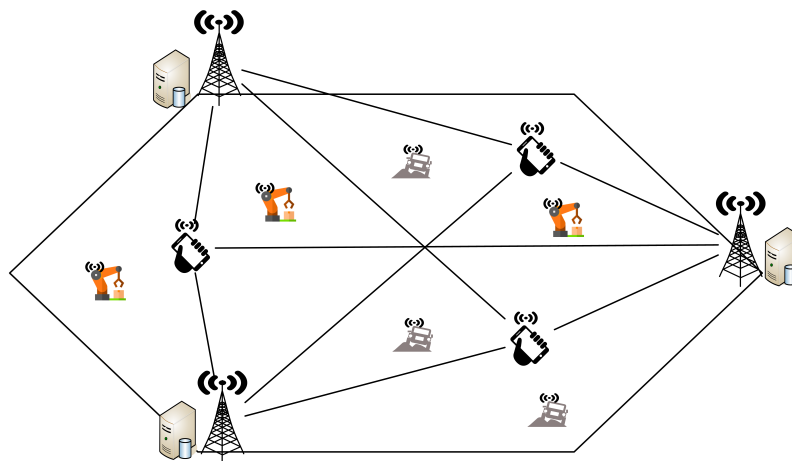


Figure 1. K -User MIMO X network Example for $K = 3$.

In any form of K -User MIMO, each mobile device receives both its desired signals and interference signals (signals meant for other mobile devices). To manage interference, K -User MIMO systems are often studied in the context of Interference Alignment (IA). IA is a technique that aligns interfering signal vectors in order to maximize interference-free space at each mobile device [11]. By applying suitable channel dependent precoders to the transmit signals, and beamformers to the receive signals, several interfering users can communicate simultaneously. Alignment helps confine the interference at each mobile device to a smaller dimensional subspace while projecting the desired signals into the null space of the interference.

Several works have analyzed IA on a theoretical level. A typical metric used to characterize IA is known as Degrees of Freedom (DoF). DoF is defined as the number of spatial dimensions that are free from interference [12]. The authors in [13] have provided examples showing achievability of IA and various DoF in K -User interference networks with different antenna configurations. In [14], an iterative algorithm for obtaining the precoders and beamformers is presented for a Time Division Duplex (TDD) mode of operation. The precoders in this method are a function of the dual relationship between the MIMO forward and reverse channels. Another IA framework involving TDD channels is presented in [15]. In [16], interference alignment in MIMO downlink networks is investigated, where precoders are derived by eigen decomposition of the MIMO channels.

Another IA scheme for a K -User MIMO X network is proposed in [17]. By appropriately precoding the transmit signals, this scheme maximizes the interference-free space by limiting the interference at every mobile device to half of the received signal space. Further, by applying a zero forcing beamformer which is a function of interfering channels and precoders, interference cancellation has been achieved for $K = 3$. The algorithms in [17] are purely theoretical and in this paper, we improve upon them.

Discussion on how to demodulate symbols is not provided in [17]. Further, in order to maximize capacity, we wish to operate the K -User MIMO X system such that each access point is transmitting different symbols to each mobile device, whilst all being on the same frequency subcarrier. We have investigated the case where each access point is on a different subcarrier in [18] and found that the

bandwidth and therefore the capacity of the K -User system is reduced by a factor of K , which is significant. This paper presents a new signal separation beamformer to regain the lost factor of K .

Interference Alignment uses precoders and beamformers that are channel dependent. Naturally, channel estimation is critical to IA [19,20]. Both [17] and our previous works [18,21,22] either consider perfect channel state information or do not consider exact channel estimation error models. Neither considers the overheads arising from transmitting pilot symbols for estimation. Park and Ko [17] assumes perfect channel state information. Yerrapragada and Kelley [18] does not explicitly estimate the channel but assumes a Cramér–Rao variance for the estimation error, which is only a lower-bound on the error. In [21], the channel is not estimated but the effects of imperfect estimation are simulated. Residual interference due to imperfect precoders and beamformers is modeled as a random variable and an expression for its distribution is provided. Yerrapragada and Kelley [22] is the first paper that introduces signal separation concepts for K -User MIMO, but it too assumes perfect channel estimation.

In this paper, we extend our previous work to provide realistic and practical capacity results for K -User MIMO X systems that account for channel estimation overheads.

2. System Model for Cellular-Based K -User MIMO

This section describes the system model for K -User MIMO X that shows transmit precoding, receive interference cancellation, and signal separation. Table 1 shows the parameters used in the key equations and derivations. Figure 2 shows the overall K -User MIMO protocol steps. Lastly, an Orthogonal Frequency Division Multiplexing (OFDM) multiple access protocol is shown. This protocol illustrates the pilot overhead resulting from serving several ($> K$) mobile devices.

Table 1. System model parameters for key derivations.

Parameter	Description	Size	For $K = 3$
M	Minimum number of antennas at each access point and mobile device	$\geq K(K-1)$	≥ 6
N_D	Number of desired signals at each mobile device	K	3
N_I	Number of interference terms at each mobile device	$K(K-1)$	6
H_{ij}	Channel matrix between access point j and mobile device i	$M \times M$	6×6
v_{ij}	Precoder vector for signal between access point j and mobile device i	$M \times 1$	6×1
s_{ij}	Symbol to be transmitted between access point j and mobile device i	1×1	1×1
w_i	Additive White Gaussian Noise (AWGN) at mobile device i	$M \times 1$	6×1
P_i^I	Matrix of aligned interference column vectors at the mobile device i	$M \times \frac{N_I}{2}$	6×3
U_i	Zero forcing beamformer matrix at mobile device i	$M \times M - \frac{N_I}{2}$	6×3
P_{ij}^D	Matrix of desired column vectors at mobile device i to isolate signal from access point j	$M - \frac{N_I}{2} \times N_D - 1$	3×2
U_{ij}	Signal Separation beamformer matrix at mobile device i to isolate signal from access point j	$M - \frac{N_I}{2} \times (N_D - 1)$	3×1
N_s	Number of recovered copies of each symbol s_{ij}	$M - \frac{N_I}{2} - (N_D - 1)$	1

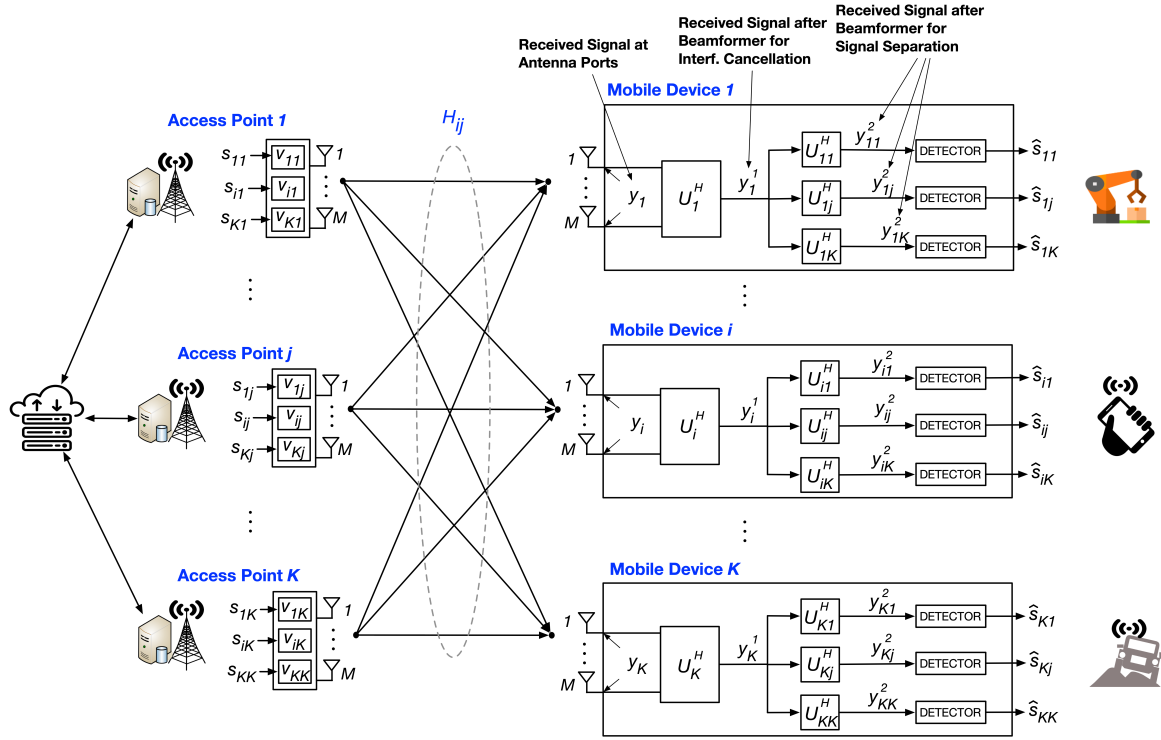


Figure 2. K -User MIMO X network showing the application of precoders at the access points as well as stage 1 and stage 2 beamformers (Equations (1)–(3)).

2.1. Received Signal at Antenna

Each of the K access points and mobile devices is equipped with M antennas. The all-to-all connectivity results in each mobile device receiving K desired signals and $K(K - 1)$ interfering signals. This is shown in Figure 2 and Equation (1). Transmitted symbols s_{ij} between the j^{th} access point and the i^{th} mobile device are precoded by length M precoder vectors v_{ij} and transmitted over Rayleigh fading channels H_{ij} . Without loss of generality, we consider downlink transmissions. The received signal at the i^{th} mobile device is given by

$$y_i = \underbrace{\sum_{j=1}^K H_{ij} v_{ij} s_{ij}}_{\text{Desired signal}} + \underbrace{\sum_{j=1}^K \sum_{k=1, k \neq i}^K H_{ij} v_{kj} s_{kj}}_{\text{Total interference}} + \underbrace{w_i}_{\text{Noise}} \quad (1)$$

This paper focuses on the maximum capacity scenario. Therefore it is assumed that each s_{ij} is unique. The precoders v_{ij} are channel dependent and are obtained by solving a system of alignment equations. The procedure for obtaining the precoder vectors is shown in Appendix A. The noise at the i^{th} mobile device, w_i is assumed to be 0 mean Additive White Gaussian Noise (AWGN) with variance $\sigma_{w_i}^2 = E[w_i w_i^*]$, where $E[\cdot]$ represents the expected value.

2.2. Received Signal after Beamformer for Interference Cancellation

A beamformer matrix U_i is applied to the received signal y_i to cancel the interference, as shown below:

$$y_i^1 = U_i^H \cdot y_i = U_i^H \sum_{j=1}^K H_{ij} v_{ij} s_{ij} + \underbrace{U_i^H \cdot \sum_{j=1}^K \sum_{k=1, k \neq i}^K H_{ij} v_{kj} s_{kj}}_{I_e \approx 0} + U_i^H w_i, \quad (2)$$

where I_e is the residual interference after cancellation. In the case of perfect channel state information, it is exactly equal to zero. The interference cancellation beamformer U_i is obtained by first generating a matrix, whose columns contain aligned interference vectors. The left-hand side of the Singular Value Decomposition (SVD) of this matrix contains the beamformer. The derivation of this beamformer is shown in Appendix A.

2.3. Received Signal after Beamformer for Desired Signals Separation

Symbols transmitted from access points on the same frequency subcarrier, add coherently at the mobile device. Under this model, symbol recovery is straightforward when each access point sends the same symbol to the i^{th} mobile device. However, for maximizing capacity, each access point must be able to send different symbols to the i^{th} mobile device. In such cases, a second beamformer operator is applied after interference cancellation, as shown in Equation (3). This second operator is applied K times at each mobile device (shown in Figure 1) and helps separate the signals sent from each of the K access points.

$$\begin{aligned} y_{ij}^2 &= U_{ij}^H U_i^H y_i^1 = U_{ij}^H U_i^H \sum_{j=1}^K H_{ij} v_{ij} s_{ij} + \underbrace{U_{ij}^H I_e + U_{ij}^H U_i^H w_i}_{\approx 0} \\ &= U_{ij}^H U_i^H H_{ij} v_{ij} s_{ij} + U_{ij}^H U_i^H w_i \xrightarrow{\text{To detector for symbol recovery}} \hat{s}_{ij}. \end{aligned} \quad (3)$$

The signal separation beamformer U_{ij} is obtained by first generating a matrix whose columns contain desired signal vectors from other access points that act as interference when recovering the symbol transmitted from a specific access point. The left-hand side of the SVD of this matrix contains the beamformer. The derivation of this beamformer is shown in Appendix A.

After separation, the desired signals from each of the K access points can be decoded by correcting for the effects of U_{ij} , U_i , H_{ij} , and v_{ij} . The decoding and detection process that recovers the symbols s_{ij} is shown in Appendix A.

2.4. K-User MIMO X Multiple Access Protocol

We now apply K -User MIMO X to a typical OFDM cellular scenario. Let us assume that there are nK mobile devices ($n \geq 1$) associating with K access points forming n K -User-Groups (UG). In a single UG, there are $K^2 M^2$ Channel Impulse Responses (CIR) that need to be estimated. We propose that each of the MK transmit antennas sends pilot symbols on non-overlapping OFDM symbol times. In this paper, we assume the use of pilot signals that are configured for both synchronization as well as channel estimation. An example of such a sequence is the Zadoff–Chu sequence, commonly used in 4G Long Term Evolution (LTE). Akin to LTE pilot signals, when one transmit antenna is sending pilots, all other transmit antennas are off. This is shown in Figure 3. In the time domain, the channel needs to remain constant for at least MK symbol times. We leverage frequency domain resources to support the n User Groups. In the frequency domain, the available bandwidth B is divided into m sub-bands, where $m = \frac{B}{B_c}$ and B_c is the channel coherence bandwidth. Each of the m sub-bands is divided equally among the n K -User-Groups. As shown in Figure 3, each UG gets a chunk of bandwidth in each of the m sub-bands in which to transmit pilot signals for synchronization and channel estimation. The channels in the sub-bands not available for a certain UG can easily be obtained by interpolation. The channel estimates are conveyed by the mobile devices to a global network entity in the backhaul which makes all channels available to all access points and mobile devices through the appropriate interfaces. The overhead from this step is not considered in this paper and will make up future work.

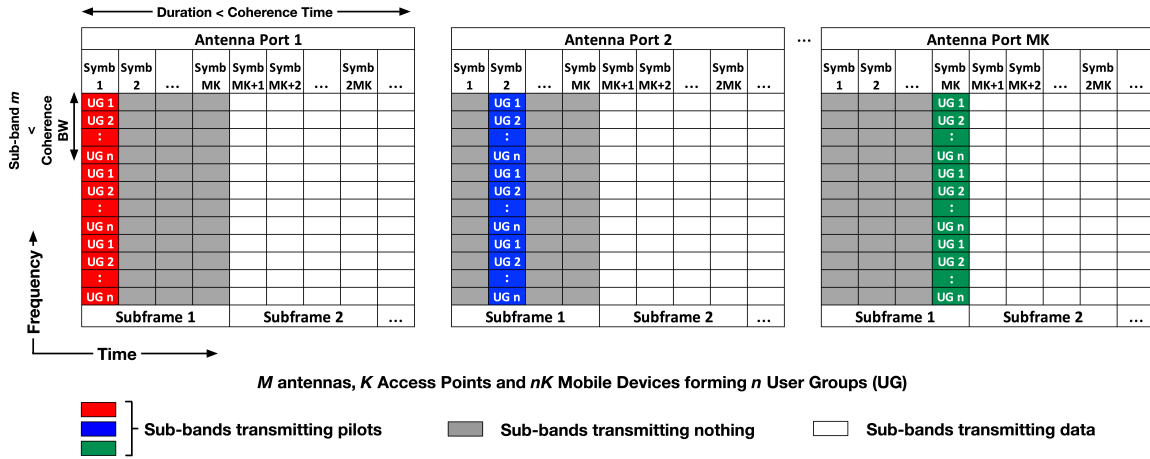


Figure 3. Example showing the channel estimation overhead for n K-User-Groups (UG). The bandwidth allocated for estimation is divided among the n K-User-Groups. Each group transmits pilot signals in its allocated band.

3. Derivation of Shannon Capacity for K-User MIMO X and Small Cell Geometric Capacity in Rayleigh Fading

This section presents an analysis of Shannon Capacity as a function of K , with and without pilot overheads. Further simulation results show the statistical distributions of capacity for $K = 3$ in Rayleigh fading and small cell geometries.

3.1. Ideal K-User MIMO X Capacity vs. K Excluding Pilot Overhead

The theorem for the upper-bound capacity for K-User MIMO X incorporates channel and beamformer gains that scale with K and antenna array size M . It is defined below.

Theorem 1. The upper bound multi-user capacity of a K-User MIMO X system is bounded by $C_{\text{bits/sec}} \leq BK^2 \log_2(1 + \left[M - \frac{N_L}{2} - (N_D - 1)\right] \left[M - \frac{N_L}{2}\right]^2 M^2 \times \text{SINR})$, where B is the bandwidth, and the $\text{SINR} = \frac{P_t d^{-\alpha}}{\sigma_w^2}$ includes the transmit power P_t and the distance dependence based on a path loss exponent α and target distance d . The proof of Theorem 1 and verification by simulation are shown in Appendices B and C, respectively. The result of Theorem 1 gives the upper-bound multi-user capacity of the combined K^2 streams. Note that the theorem represents an unconstrained case which assumes that the entire available time-frequency resources are available only for data transmission.

3.2. Ideal K-User MIMO X Capacity vs. K Including Pilot Overhead

Real systems are impacted by various overheads for synchronization signals, channel estimation pilot signals, and exchange of other control information. In this paper, we consider two of the most important overheads—that of synchronization and channel estimation. We propose the use of pilot signals configured for both time synchronization and channel estimation. Consequently, we define the following theorem that refines Theorem 1 to include pilot overheads.

Theorem 2. If MK channel estimation symbols can be transmitted in less than the channel coherence time, i.e., $MKT_{\text{symp}} < T_c$, the remaining time can be reserved exclusively for data transmission. The capacity equation in Theorem 1 can be modified as follows, $C_{\text{bits/sec}} \leq \frac{T_c - MKT_{\text{symp}}}{T_c} BK^2 \log_2(1 + \left[M - \frac{N_L}{2} - (N_D - 1)\right] \left[M - \frac{N_L}{2}\right]^2 M^2 \times \text{SINR})$, where T_c is the channel coherence time. T_{symp} is the duration of 1 OFDM symbol given

by $(N + CP)T_s$, where N is the size of the Fast Fourier Transform (FFT), CP is the size of the Cyclic Prefix in samples, and T_s is the sampling period.

Figure 4 shows the Shannon Capacity curves for K -User MIMO X with and without pilot overheads. The key observation from the curves is that while the unconstrained capacity from Theorem 1 continues to grow with K , that is not the case when pilot overheads are taken into account. After a certain point, it can be seen that the pilot overheads overwhelm the gains from K -User MIMO and the capacity begins to drop. In highly varying channel scenarios, it is more beneficial to operate at a lower value of K and schedule several User Groups in a multiple access framework similar to that shown in Figure 3. Figure 4 also compares the performance of our K -User MIMO X system with 5G-NR Massive MIMO [23]. It should be noted that the Massive MIMO model assumes one access point equipped with M antennas and K single-antenna mobile devices. The Shannon limit is also plotted. This limit is based on the analysis provided in [24] and assumes a system with a single access point and single mobile device each with MK antennas.

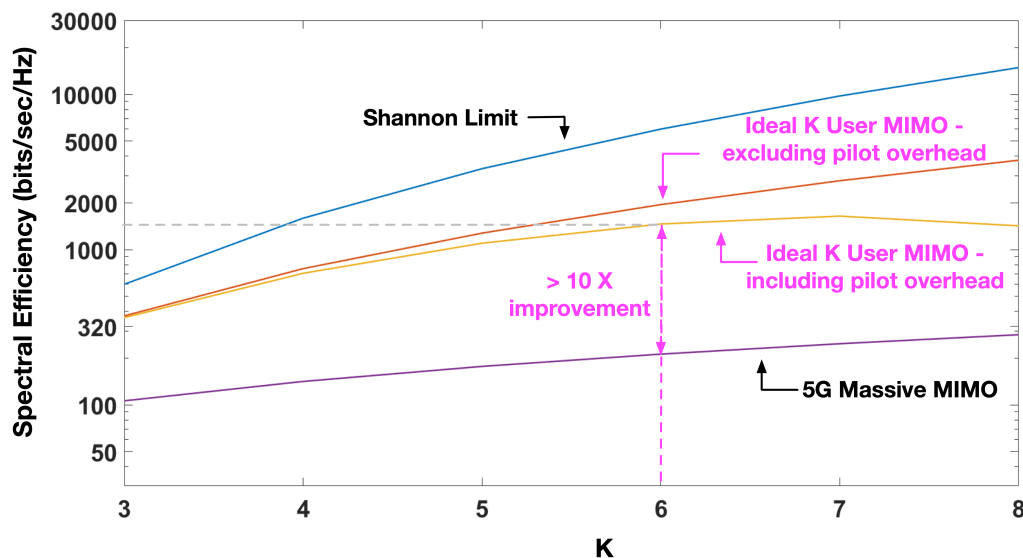


Figure 4. Comparison of our very high throughput K -User MIMO X spectral efficiencies against related technologies such as 5G-NR Massive MIMO. Spectral Efficiencies are for a 100 m cell in an Indoor A channel scenario. The curve for Massive MIMO is based on the formula shown in [23]. The number of antennas is $M = K(K - 1)$.

3.3. Capacity Results for Small Cell K -User MIMO at $K = 3$

This section describes the simulation model, choosing $K = 3$ as an example. Simulations are done in MATLAB and the key parameters are listed in Table 2. Cell spectral efficiency performance in 500 m, 100 m, and 50 m hexagonal cells is obtained and shown in Figure 5.

Table 2. Simulation Parameters.

Channel Model	Rayleigh Fading
Channel Scenario	Indoor A [25]
Cell Radius	50 m, 100 m, 500 m
Transmit Power	16 dBW
Total Bandwidth	20 MHz
FFT Size (N)	2048
Cyclic Prefix (CP)	512 samples
Sampling frequency	30.72 MHz
Subcarrier spacing	15 kHz
Number of used sub-carriers	1320
Noise Figure	4 dB
Thermal Noise Density	−203.9 dBW/Hz
Path Loss Exponent	3

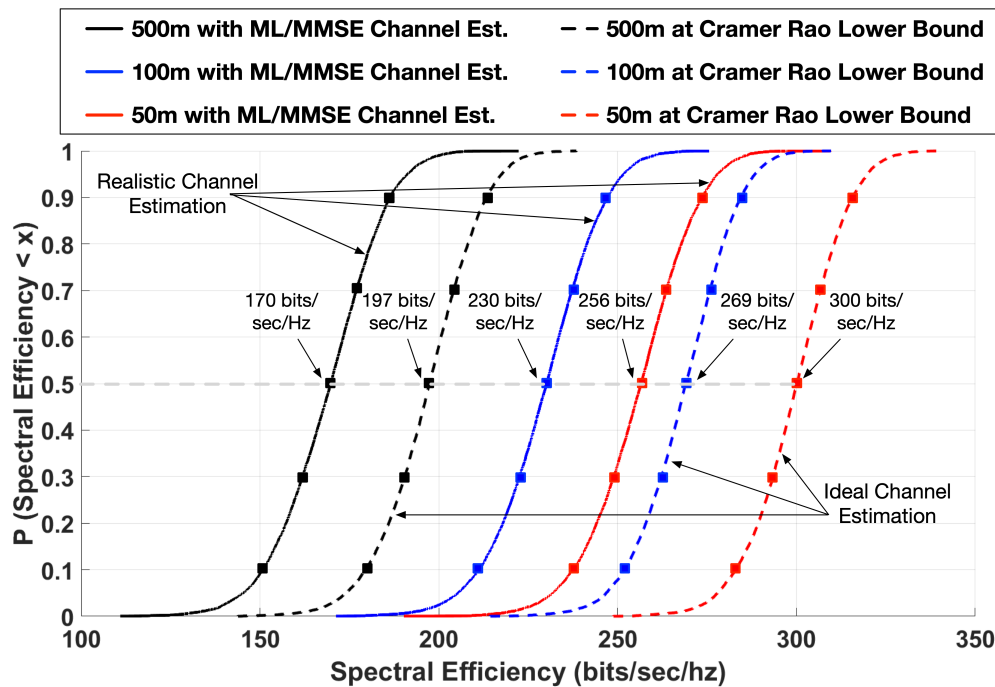


Figure 5. Cumulative distribution functions of spectral efficiencies in bits/sec/Hz for $K = 3$ in single hexagonal cells of radius 50 m, 100 m, and 500 m for Indoor A channel scenarios [25]. Results are shown both with realistic channel estimation using ML/MMSE and also at the Cramér–Rao Lower Bound.

Without loss of generality, the hexagonal geometry is chosen, for simplicity of analysis. The system can easily be translated to stochastic geometries, commonly associated with 5G systems. 3 access points are placed on alternate corners of the cell. 3 mobile devices are placed uniformly within the cell. The simulations assume an exponential path loss $L_{ij} = d_{ij}^{-\alpha}$.

While K -User MIMO X is not limited by any particular channel scenario, we note that one example of a use case is a high-throughput IoT robotic factory model. Hence, without loss of generality, a Rayleigh fading channel model with the Indoor A power delay profile [25] is used. Considering an Indoor A channel scenario with parameters such as velocity $v = 3$ kmph, carrier frequency $f_c = 1.9$ GHz, and speed of light $c = 3 \times 10^8$ m/s, the channel coherence time T_c is calculated as $T_c = \sqrt{\frac{9}{16\pi f_d^2}} \approx 80$ ms, where f_d is the Doppler shift given by $f_d = \frac{vf_c}{c}$. Let us assume that we only have a fraction of the channel coherence time, say 60 ms.

Multiple channel and location trials are run. In each trial, the channel is estimated in the first 18 symbol times (1.5 ms). This paper assumes the use of well-known estimation methods such as the Maximum Likelihood (ML) or Minimum Mean Square Error (MMSE).

For statistical analysis, it suffices to assume the presence of one K -User-Group. In such a case, the entire bandwidth is available for pilot signals. We use the Zadoff–Chu sequence for both time synchronization and channel estimation. After channel estimation, the remaining 58.5 ms is available for data transmission. The Cumulative Distribution Function (CDF) of the spectral efficiency is calculated from the multiple trials and plotted in Figure 5. These spectral efficiencies account for pilot signal overhead as well as estimation error.

In the case of $n > 1$ K -User-Groups, in the channel estimation symbols, the bandwidth can be divided as shown in Figure 3. In the data transmission symbols, the bandwidth could also be divided into sub-bands in which the different User Groups could be network scheduled using greedy or proportional fair algorithms.

Incorporation of Channel Estimation Errors

Figure 6 shows the variance of the estimation error as a function of signal-to-noise ratio for both the ML and MMSE estimates. The Cramér–Rao Lower Bound (CRLB) is also shown. As expected, the ML and MMSE variances are higher than the CRLB. The equations for the channel estimation methods and the CRLB are well researched in other works and are hence shown in Appendix D. Figure 5 also shows the spectral efficiency if the estimation error variance is at the Cramér–Rao Lower Bound (CRLB). To simulate this, we calculate the CRLB as shown in Equation (A15) in Appendix D. The CRLB is calculated for each transmit–receive antenna link, and error terms are drawn from $\mathcal{CN}(0, \sigma_{CRLB}^2)$. These errors are added to the actual channels to simulate estimation error at the CRLB.

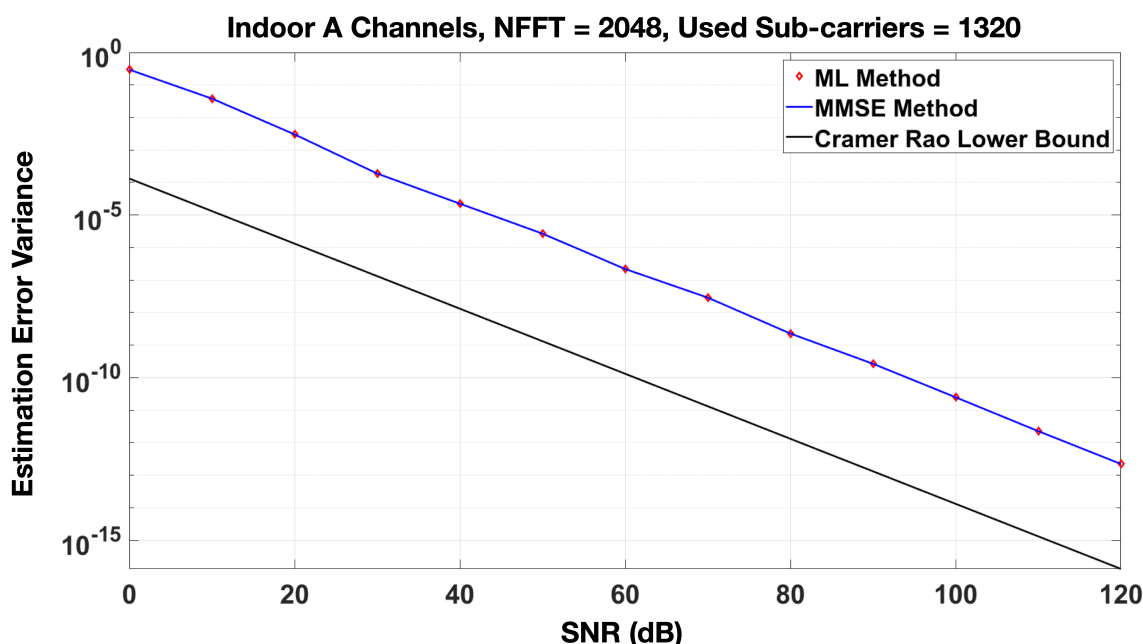


Figure 6. Comparison of channel estimation error variance between Maximum Likelihood (ML)/Minimum Mean Square Error (MMSE) and the Cramér–Rao Lower Bound (CRLB).

It can be seen from Figure 5 that the median best case spectral efficiency in 500 m, 100 m, and 50 m cells are 170, 230, and 256 bits/sec/Hz, respectively. These results are under Rayleigh fading conditions. If the channel follows a Rician distribution, it means that there is one dominant line of sight path in the Channel Impulse Response. The stronger the line-of-sight component, the rarer the occurrences of deep fades. Though this scenario is not simulated explicitly, we have investigated another scenario which is

maximum capacity scheduling with Rayleigh fading. This approach schedules K -User-Groups in a particular sub-band with the best channel conditions, thus weeding out deep fade channel instances. We have found very little improvement in spectral efficiency with this type of scheduling. We believe that the same will be the case with Rician channels. The reason for this is that the non co-located nature of K -User MIMO transmitters already provides enough channel diversity to overcome the effects of deep fades.

The spectral efficiencies in Figure 5 are multi-user values and take into account the fact that channel estimation through pilot signals takes up 18 symbol times, where no data is transmitted. In a 20 MHz band, this amounts to a best-case scenario of 3.4 Gbps, 4.6 Gbps, and 5.1 Gbps, respectively; and in the case of 5 aggregated bands, data rates in excess of 17 Gbps, 23 Gbps, and 25 Gbps, respectively, can be achieved. This underlines the wide range of exciting possibilities that can be achieved in beyond-5G and 6G networks with K -User MIMO X.

The 6G extension of eMBB, defined in [26] as eMBB Plus, will serve mobile and IoT communications with data rate requirements far greater than 5G. The high throughput and spectral efficiency of K -User MIMO X lend themselves well to help support eMBB Plus. 6G will also be more machine-learning and security driven [27,28]. The all-to-all nature of K -User MIMO X, with its ability to switch between maximum capacity and maximum reliability modes, makes it particularly suitable for future machine learning integration. Machine learning algorithms could be used to come up with new encoding schemes across the K transmitters that can help adapt to spatially and temporally varying channel conditions as well as eavesdroppers and jammers. This flexibility leads perfectly into the 6G version of URLLC, known as event-defined-URLLC [28], which provides context-aware communications not thought of in 5G.

4. Conclusions

In this paper, we have reviewed and identified the massive scope for increased throughput for beyond-5G or 6G networks. Under realistic channel estimation constraints, we have provided a K -User MIMO X framework that can cancel interference, demodulate, and maximize capacity through signal separation. Further practical aspects such as OFDM multiple access for channel estimation and data transmission have been described. Lastly, cell capacity performance has been simulated and compared with related technologies.

Author Contributions: Conceptualization, A.K.Y. and B.K.; investigation, A.K.Y.; methodology, A.K.Y. and B.K.; writing—original draft, A.K.Y.; writing—review and editing, A.K.Y. and B.K. All authors have read and agreed to the published version of the manuscript.

Funding: This research was funded by US Air Force Research Laboratory and Office of the Secretary of Defense under Testing, Evaluation, and Control of Heterogeneous Large Scale systems of Autonomous Vehicles (TECHLAV) with grant number FA8750-15-2-0016.

Conflicts of Interest: The authors declare no conflict of interest.

Appendix A. K -User MIMO Interference Alignment Mathematics for $K = 3$

Appendix A.1. System of Interference Alignment Equations for Precoder Generation

Interference cancellation can be achieved subject to the following constraints.

Postulate 1 [17]: At each mobile device, interfering signals from the same access point cannot be aligned in the same direction such that $H_{ij}v_{kj} \neq H_{ij}v_{lj}$, where $i \neq k \neq l$.

Postulate 2 [17]: In a K user system, since each mobile device receives $K(K - 1)$ interference components, in order to align $(K - 1)$ interference signals along K dimensions, the condition to be met is $\text{span}(H_{im}v_{km}) = \text{span}(H_{in}v_{ln})$, where $k, l \neq i$.

Since there are $K(K - 1)$ interference terms at each mobile device, the minimum number of antennas at each access point and mobile device has to be $M = K(K - 1)$.

Table A1 shows one possible set of Interference Alignment equations for $K = 3$. These equations are formed by dividing the $K(K - 1)$ interference terms at each mobile device into pairs, subject to postulates 1 and 2. Each pair represents the left- and right-hand sides of a single IA equation. Since there are $K(K - 1)$ interference terms at each mobile device, there will be $\frac{K(K-1)}{2}$ IA equations. These equations will be used to solve for the precoders.

Table A1. K -User MIMO X Interference Alignment (IA) conditions, $K = 3$.

	IA conditions [17]
Rx 1	$\text{span}(H_{11}v_{21}) = \text{span}(H_{12}v_{22})$
	$\text{span}(H_{11}v_{31}) = \text{span}(H_{13}v_{33})$
	$\text{span}(H_{12}v_{32}) = \text{span}(H_{13}v_{23})$
Rx 2	$\text{span}(H_{21}v_{11}) = \text{span}(H_{22}v_{12})$
	$\text{span}(H_{21}v_{31}) = \text{span}(H_{23}v_{13})$
	$\text{span}(H_{22}v_{32}) = \text{span}(H_{23}v_{33})$
Rx 3	$\text{span}(H_{31}v_{11}) = \text{span}(H_{33}v_{23})$
	$\text{span}(H_{31}v_{21}) = \text{span}(H_{32}v_{12})$
	$\text{span}(H_{32}v_{22}) = \text{span}(H_{33}v_{13})$

Each access point will apply K precoders. From the IA equations, the precoders v_{ij} are obtained as follows:

$$\begin{aligned}
 v_{12} &= (H_{22})^{-1}H_{21}v_{11} & v_{33} &= (H_{13})^{-1}H_{11}v_{31} \\
 v_{21} &= (H_{31})^{-1}H_{32}v_{12} & v_{32} &= (H_{22})^{-1}H_{23}v_{33} \\
 v_{22} &= (H_{12})^{-1}H_{11}v_{21} & v_{23} &= (H_{13})^{-1}H_{12}v_{32} \\
 v_{13} &= (H_{33})^{-1}H_{32}v_{22} & v_{11} &= (H_{31})^{-1}H_{33}v_{23} \\
 v_{31} &= (H_{21})^{-1}H_{23}v_{13}.
 \end{aligned} \tag{A1}$$

The initial value of v_{11} is obtained by first defining a matrix E [17] as follows:

$$\begin{aligned}
 E &= (H_{31})^{-1}H_{33}(H_{13})^{-1}H_{12}(H_{22})^{-1}H_{23}(H_{13})^{-1}H_{11} \\
 &\times (H_{21})^{-1}H_{23}(H_{33})^{-1}H_{32}(H_{12})^{-1}H_{11}(H_{31})^{-1}H_{32} \\
 &\times (H_{22})^{-1}H_{21}.
 \end{aligned} \tag{A2}$$

It is to be noted that E is obtained from Equation (A1). Then, v_{11} is arbitrarily chosen to be one of the eigenvectors of E and subsequently, all the other precoders can be obtained in the order, v_{12} , v_{21} , v_{22} , v_{13} , v_{31} , v_{33} , v_{32} , and v_{23} .

Appendix A.2. Obtaining the Beamformer for Interference Cancellation

The zero forcing beamformer matrix U_i is obtained by first defining a matrix P_i^I for each mobile device and taking the Singular Value Decomposition (SVD) as follows:

$$\begin{aligned}
 P_1^I &= \begin{bmatrix} H_{11}v_{21} & H_{11}v_{31} & H_{12}v_{32} \end{bmatrix} \\
 &= \begin{bmatrix} \bar{U}_1^{(1)} & \bar{U}_1^{(0)} \end{bmatrix} \begin{bmatrix} \bar{\Lambda}_1 \\ 0 \end{bmatrix} \begin{bmatrix} \bar{V}_1^{(1)} & \bar{V}_1^{(0)} \end{bmatrix}^H,
 \end{aligned} \tag{A3}$$

where P_1^I is the set of aligned interfering column vectors at the first mobile device. From Equation (A3), we can set $\bar{U}_1^{(0)} = U_1$, the zero forcing beamformer at the first mobile device. The number of

columns in U_1 is equal to the number of nonzero singular values in $\bar{\Lambda}_1$. Similarly, we determine the beamformers at the second and third mobile devices by defining $P_2^I = \begin{bmatrix} H_{21}v_{11} & H_{21}v_{31} & H_{22}v_{32} \end{bmatrix}$ and $P_3^I = \begin{bmatrix} H_{31}v_{11} & H_{31}v_{21} & H_{32}v_{22} \end{bmatrix}$, where P_2^I and P_3^I are the sets of aligned interfering column vectors at the second and third mobile devices, respectively.

Appendix A.3. Obtaining the Beamformer for Signal Separation

At the i^{th} mobile device, in order to separate the different signals sent from the K access points, we apply a second beamformer matrix. This operator is applied K times at each mobile device. This matrix is obtained by defining a matrix P_{ij}^D for each access-point–mobile-device pair and taking the SVD as follows:

$$\begin{aligned} P_{11}^D &= \begin{bmatrix} U_1^H H_{12} v_{12} & U_1^H H_{13} v_{13} \end{bmatrix} \\ &= \begin{bmatrix} \bar{U}_{11}^{(1)} & \bar{U}_{11}^{(0)} \end{bmatrix} \begin{bmatrix} \bar{\Lambda}_{11} \\ 0 \end{bmatrix} \begin{bmatrix} \bar{V}_{11}^{(1)} & \bar{V}_{11}^{(0)} \end{bmatrix}^H, \end{aligned} \quad (A4)$$

where P_{11}^D is the set of desired column vectors at mobile device 1 corresponding to access points 2 and 3. From Equation (A4), we can set $\bar{U}_{11}^{(0)} = U_{11}$. The number of columns in U_{11} is equal to the number of nonzero singular values in $\bar{\Lambda}_{11}$. The matrix U_{11} , when multiplied to the received signal after zero forcing, isolates the desired signal at mobile device 1 from access point 1. Similarly, the desired signals at mobile device 1 from access points 2 and 3 respectively can be isolated by defining $P_{12}^D = \begin{bmatrix} U_1^H H_{11} v_{11} & U_1^H H_{13} v_{13} \end{bmatrix}$ and $P_{13}^D = \begin{bmatrix} U_1^H H_{11} v_{11} & U_1^H H_{12} v_{12} \end{bmatrix}$, where P_{12}^D and P_{13}^D are the sets of desired column vectors at mobile device 1 corresponding to access points 1,3 and 1,2, respectively. The same process can be repeated at the other mobile devices.

Appendix A.4. K-User MIMO X Demodulation and Symbol Detection

The following demodulation process helps recover symbols arriving from each access point. Note that this process is applied after zero forcing and signal separation. Defining $\Gamma_{ij} = U_{ij}^H U_i^H H_{ij}$ and taking the SVD, we have

$$\Gamma_{ij} = \Phi_{ij} \cdot \Lambda_{ij} \cdot \Psi_{ij}^H, \quad (A5)$$

where Λ_{ij} is a diagonal matrix containing the singular values of Γ_{ij} such that

$$\Lambda_{ij} = \begin{bmatrix} \lambda_{ij}(1) & 0 & \dots & 0 & 0 & 0 \\ 0 & \lambda_{ij}(2) & 0 & \dots & 0 & 0 \\ \vdots & \vdots & & & \ddots & \\ 0 & 0 & \lambda_{ij}(N_s) & 0 & \dots & 0 \end{bmatrix}. \quad (A6)$$

The information symbol from access point j to mobile device i is estimated by the element wise division,

$$[\hat{s}_{ij}(1), \dots, \hat{s}_{ij}(\gamma), \dots, \hat{s}_{ij}(N_s)]^T = \frac{\phi_{ij}^H \tilde{y}_{ij}}{\psi_{ij}^H v_{ij}}. \quad (A7)$$

The demodulation process recovers N_s copies (refer to Table 1) of each symbol s_{ij} corresponding to the number of nonzero singular values in Λ_{ij} .

Due to interference cancellation, the demodulated signal obtained from Equation (A7) takes the form

$$\hat{s}_{ij} = \sum_{\gamma=1}^{N_s} \lambda_{ij}(\gamma) s_{ij}(\gamma) + \hat{w}_i, \quad (A8)$$

where $\lambda_{ij}(\gamma)$ is the γ^{th} diagonal element in Λ_{ij} and \hat{w}_{ij} is the noise after demodulation.

The spectral efficiency after interference cancellation, signal separation, and demodulation can be computed as follows:

$$C_{bits/sec/Hz} = \log_2 \left[1 + \frac{\left| \sum_{\gamma=1}^{N_s} \lambda_{ij}(\gamma) s_{ij}(\gamma) \right|^2}{|\hat{w}_{ij}|^2} \right]. \quad (A9)$$

Appendix B. Proof of Theorem 1

Proof. To complete the proof, we leverage two well-known results from Matrix Theory [29]. First, for any matrix A , the sum of the squares of the singular values is equal to the square of its Frobenius Norm such that $\sum_i \lambda_i^2(A) = \|A\|_F^2$, where $\lambda_i(A)$ is the i^{th} singular value of A and $\|A\|_F$ is the Frobenius Norm of A . This follows from the decomposition of matrix A as a singular value decomposition, $A = U\Lambda V^H$. The Frobenius norm is invariant under orthogonal transformation of the left and right orthogonal matrices. Therefore, based on the fact that $\lambda_i(A)$ is the component of A along the diagonal of Λ , the sum of squares of the components of Λ equals the square of the Frobenius norm.

Second, the Frobenius Norm of the product of matrices is upper bounded by the product of the Frobenius Norms of the individual matrices such that $\|AB\|_F \leq \|A\|_F \|B\|_F$. The proof of this is based on the well-known Cauchy–Schwarz Inequality.

From Equation (A5), $\Gamma_{ij} = U_{ij}^H U_i^H H_{ij}$ and $\lambda_{ij}(1) \cdots \lambda_{ij}(N_s)$ are the singular values of Γ_{ij} . Combining the above two statements from [29],

$$\begin{aligned} \sum_{\gamma=1}^{N_s} |\lambda_{ij}(\gamma)|^2 &= \|\Gamma_{ij}\|_F^2 \\ &\leq \|U_{ij}^H\|_F^2 \|U_i^H\|_F^2 \|H_{ij}\|_F^2 \\ &\leq \sum |\lambda(U_{ij}^H)|^2 \sum |\lambda(U_i^H)|^2 \sum |\lambda(H_{ij})|^2 \\ &\leq \left[M - \frac{N_I}{2} - (N_D - 1) \right] \left[M - \frac{N_I}{2} \right] \cdot \left[M - \frac{N_I}{2} \right] M \cdot M, \end{aligned} \quad (A10)$$

where $\lambda(U_{ij}^H)$, $\lambda(U_i^H)$, and $\lambda(H_{ij})$ are the singular values of U_{ij}^H , U_i^H , and H_{ij} , respectively. It should be noted that $\sum_{\gamma=1}^{N_s} |\lambda_{ij}(\gamma)|^2$ is the gain for one stream between the j^{th} access point and the i^{th} mobile device. There are K^2 such streams. Therefore, the multi-user capacity is given by

$$C_{bits/sec} \leq BK^2 \log_2 \left(1 + \left[M - \frac{N_I}{2} - (N_D - 1) \right] \left[M - \frac{N_I}{2} \right]^2 M^2 \times SINR \right). \quad (A11)$$

□

Appendix C. Verification of Capacity Upper Bound

To verify the capacity upper bound for $K = 3$, several simulation trials were run in which Rayleigh Fading Channels with the Indoor A power delay profile were generated. It should be noted that U_{ij} and U_i are normalized to have a power of 1, whereas H_{ij} has a power of 1 only in an expected sense. The values of $\sum |\lambda(U_{ij}^H)|^2$, $\sum |\lambda(U_i^H)|^2$, and $\sum |\lambda(H_{ij})|^2$ were found to be 3, 18, and 6, which correspond to the dimensions of U_{ij} , U_i , and H_{ij} , respectively (Table 1).

The SVD in Equation (A5) is computed and a distribution of the sum of the singular value powers $\sum_{\gamma=1}^{N_s} |\lambda_{ij}(\gamma)|^2$ is plotted. This is shown in Figure A1. It can be clearly seen from the distribution that the values of the singular value power sum fall below the upper bound for $K = 3$, thus satisfying the theorem.

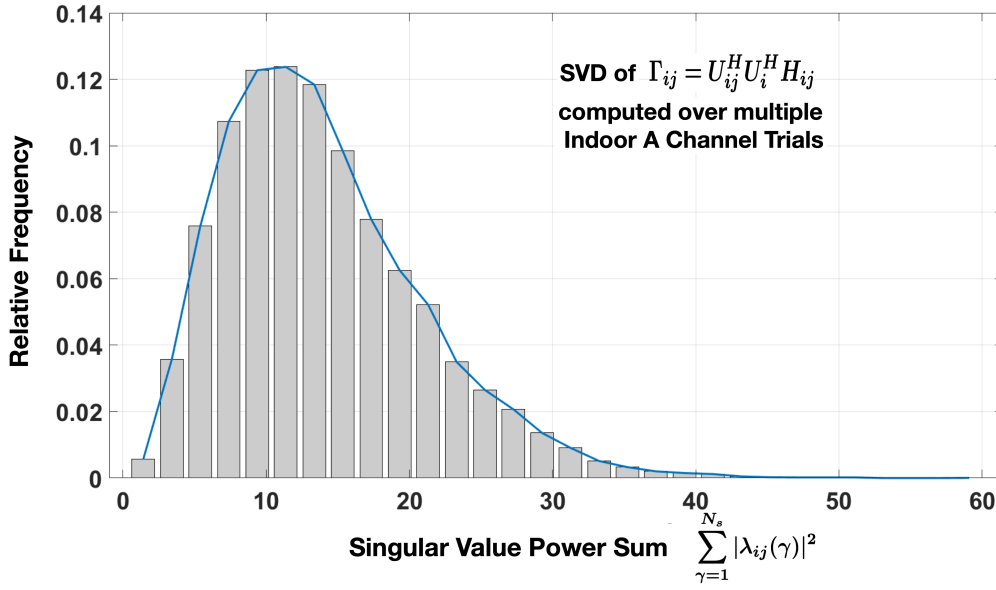


Figure A1. Relative frequency distribution of the singular value power sum for $K = 3$. The upper bound for this sum is given by Equation (A10).

Appendix D. Channel Estimation Theory and Cramér–Rao Lower Bound

In OFDM systems, for proper detection of symbols, channel estimation is performed by transmitting either known pilot symbols at certain frequency subcarriers or across the entire OFDM symbol. In the K -User MIMO X framework described above, the pilot signals are set up such that only one antenna is transmitting in any given symbol time, during the estimation phase. So, the MIMO channel estimation can be broken down into several single-antenna channel estimations. To that end, in this section, we summarize some of the well known theories on estimating a channel between a single transmit–receive antenna pair. We also present the mathematics for calculating the Cramér–Rao Lower Bound (CRLB).

Let $h = [h(0), h(1), \dots, h(L-1)]^T$ represent the length L Channel Impulse Response (CIR). Let us denote the Channel Frequency Response (CFR) as $H = Fh$, where F is the $N \times N$ Fourier Transform twiddle factor matrix, where N is the Fourier Transform size.

Let us assume that an OFDM symbol X containing N_p pilots is transmitted, where $N_p \leq N$. The received signal Y between a single transmit–receive antenna pair in the frequency domain is given by [30]

$$Y = \text{diag}(X)Fh + W, \quad (\text{A12})$$

where W is the noise with variance σ_w^2 .

Let F_p denote the $N_p \times L$ truncated Fourier matrix. The Maximum Likelihood estimate of the channel is given by [30]

$$h_{ML} = (F_p^H F_p)^{-1} F_p^H \text{diag}(X)^H Y. \quad (\text{A13})$$

It is to be noted that h_{ML} is in the time domain. The corresponding frequency domain estimate H_{ML} can be obtained by taking the Fourier Transform.

The Minimum Mean Square Error estimate of the channel is given by [30]

$$H_{MMSE} = R_{HH_p} (R_{HH_p} + \sigma^2 (\text{diag}(X) \text{diag}(X)^H)^{-1})^{-1} H_{ML}, \quad (\text{A14})$$

where H_p is the channel frequency response at the pilot subcarriers, R_{HH_p} is the cross-correlation between all the subcarriers and the pilot-subcarriers, and $R_{H_p H_p}$ is the autocorrelation between the pilot subcarriers.

The CRLB is referenced from [31], in which it is defined as follows:

$$\sigma_{\text{CRLB}}^2 = \sigma^2 \text{Tr}\{D^{-1}\}, \quad (\text{A15})$$

where $\frac{1}{\sigma^2}$ is the effective signal-to-noise ratio after the signal power has been normalized to 1. The operator $\text{Tr}\{\cdot\}$ is the matrix trace. The matrix D , a function of the pilot locations is defined as $D_{n,k} = \sum_{m=0}^{N_p-1} e^{-j2\pi(n-k)i_m/N}$ $0 \leq n, k \leq L-1$, where $\{i_m : 0 < m < N_p - 1\}$ represents the indices of the pilot locations.

References

- Breivold, H.P.; Sandström, K. Internet of Things for Industrial Automation—Challenges and Technical Solutions. In Proceedings of the 2015 IEEE International Conference on Data Science and Data Intensive Systems, Sydney, Australia, 11–13 December 2015; pp. 532–539.
- Yaqoob, I.; Ahmed, E.; Hashem, I.A.T.; Ahmed, A.I.A.; Gani, A.; Imran, M.; Guizani, M. Internet of things architecture: Recent advances, taxonomy, requirements, and open challenges. *IEEE Wirel. Commun.* **2017**, *24*, 10–16. [CrossRef]
- Jaber, M.; Imran, M.A.; Tafazolli, R.; Tukmanov, A. 5G Backhaul Challenges and Emerging Research Directions: A Survey. *IEEE Access* **2016**, *4*, 1743–1766. [CrossRef]
- Ishii, H.; Kishiyama, Y.; Takahashi, H. A Novel Architecture for LTE-B: C-plane/U-plane Split and Phantom Cell Concept. In Proceedings of the 2012 IEEE Globecom Workshops, Anaheim, CA, USA, 3–7 December 2012; pp. 624–630.
- Zheng, K.; Zhao, L.; Mei, J.; Dohler, M.; Xiang, W.; Peng, Y. 10 Gb/s Hetsnets with Millimeter-Wave Communications: Access and Networking-Challenges and Protocols. *IEEE Commun. Mag.* **2015**, *53*, 222–231. [CrossRef]
- Pi, Z.; Choi, J.; Heath, R. Millimeter-Wave Gigabit Broadband Evolution Toward 5G: Fixed Access and Backhaul. *IEEE Commun. Mag.* **2016**, *54*, 138–144. [CrossRef]
- Hou, X.; Wang, X.; Jiang, H.; Kayama, H. Investigation of Massive MIMO in Dense Small Cell Deployment for 5G. In Proceedings of the Investigation of Massive MIMO in Dense Small Cell Deployment for 5G, Montreal, QC, Canada, 18–21 September 2016; pp. 1–6.
- Agiwal, M.; Roy, A.; Saxena, N. Next Generation 5G Wireless Networks: A Comprehensive Survey. *IEEE Commun. Surv. Tutor.* **2016**, *18*, 1617–1655. [CrossRef]
- Lee, S.R.; Moon, S.H.; Kong, H.B.; Lee, I. Optimal Beamforming Schemes and its Capacity Behavior for Downlink Distributed Antenna Systems. *IEEE Trans. Wirel. Commun.* **2013**, *12*, 2578–2587. [CrossRef]
- Heath, R.; Wu, T.; Kwon, Y.; Soong, A. multi-user MIMO in Distributed Antenna Systems. In Proceedings of the 2010 Conference Record of the Forty Fourth Asilomar Conference on Signals, Systems and Computers, Pacific Grove, CA, USA, 7–10 November 2010; pp. 1202–1206.
- Talebi, F. A Tutorial on Interference Alignment. Available online: https://www.researchgate.net/publication/255670668_A_Tutorial_on_Interference_Alignment (accessed on 5 June 2011).
- Yetis, C.M.; Gou, T.; Jafar, S.A.; Kayran, A.H. On Feasibility of Interference Alignment in MIMO Interference Networks. *IEEE Trans. Signal Process.* **2010**, *58*, 4771–4782. [CrossRef]
- Cadambe, V.R.; Jafar, S.A. Interference Alignment and Degrees of Freedom of the K-user Interference Channel. *IEEE Trans. Inf. Theory* **2008**, *54*, 3425–3441. [CrossRef]
- Gomadam, K.; Cadambe, V.R.; Jafar, S.A. Approaching the Capacity of Wireless Networks Through Distributed Interference Alignment. In Proceedings of the IEEE GLOBECOM 2008–2008 IEEE Global Telecommunications Conference, New Orleans, LO, USA, 30 November–4 December 2008; pp. 1–6.
- Sudheesh, P.; Magarini, M.; Muthuchidambaramanathan, P. Interference Alignment for the K-user MIMO X Network Using Time Division Multiple Access. In Proceedings of the 2016 IEEE Distributed Computing, VLSI, Electrical Circuits and Robotics (DISCOVER), Mangalore, India, 13–14 August 2016; pp. 123–127.

16. Liu, W.; Sun, J.X.; Li, J.; Ma, Y. Interference Alignment for MIMO Downlink Multicell Networks. *IEEE Trans. Veh. Technol.* **2016**, *65*, 6159–6167. [[CrossRef](#)]
17. Park, S.H.; Ko, Y.C. K-user MIMO X Network System With Perfect Interference Alignment. In Proceedings of the 2011 IEEE International Conference on Communications (ICC), Kyoto, Japan, 5–9 June 2011; pp. 1–5.
18. Yerrapragada, A.K.; Kelley, B. Design of K-user massive MIMO networks. In Proceedings of the 2017 IEEE 8th Annual Ubiquitous Computing, Electronics and Mobile Communication Conference (UEMCON), New York, NY, USA, 19–21 October 2017; pp. 377–383.
19. El Ayach, O.; Lozano, A.; Heath, R.W. On the overhead of interference alignment: Training, feedback, and cooperation. *IEEE Trans. Wirel. Commun.* **2012**, *11*, 4192–4203. [[CrossRef](#)]
20. Mungara, R.K.; George, G.; Lozano, A. Overhead and spectral efficiency of pilot-assisted interference alignment in time-selective fading channels. *IEEE Trans. Wirel. Commun.* **2014**, *13*, 4884–4895. [[CrossRef](#)]
21. Yerrapragada, A.; Kelley, B. An IoT Self Organizing Network for 5G Dense Network Interference Alignment. In Proceedings of the 2017 12th System of Systems Engineering Conference (SoSE), Waikoloa, HI, USA, 18–21 June 2017; pp. 1–6.
22. Yerrapragada, A.K.; Kelley, B. Very High Throughput Internet of Things Networks with K access points and K devices. In Proceedings of the MILCOM 2019–2019 IEEE Military Communications Conference (MILCOM), Norfolk, VA, USA, 12–14 November 2019; pp. 640–645.
23. Marzetta, T.L. Massive MIMO: An introduction. *Bell Labs Tech. J.* **2015**, *20*, 11–22. [[CrossRef](#)]
24. Juntti, M. Capacity Limits of MIMO Channels. *IEEE J. Sel. Areas Commun.* **2003**, *21*, 684–702.
25. Medbo, J. Channel models for HIPERLAN/2 in different indoor scenarios. *ETSI/BRAN* **1998**, *3ERI085B*, 1–8.
26. Dang, S.; Amin, O.; Shihada, B.; Alouini, M.S. What should 6G be? *Nat. Electron* **2020**, *3*, 20–29. [[CrossRef](#)]
27. Yang, P.; Xiao, Y.; Xiao, M.; Li, S. 6G wireless communications: Vision and potential techniques. *IEEE Netw.* **2019**, *33*, 70–75. [[CrossRef](#)]
28. Letaief, K.B.; Chen, W.; Shi, Y.; Zhang, J.; Zhang, Y.J.A. The roadmap to 6G: AI empowered wireless networks. *IEEE Commun. Mag.* **2019**, *57*, 84–90. [[CrossRef](#)]
29. Golub, G.H.; Van Loan, C.F. *Matrix Computations*; JHU Press: Baltimore, MD, USA, 2012; Volume 3.
30. Ozdemir, M.K.; Arslan, H. Channel estimation for wireless OFDM systems. *IEEE Commun. Surv. Tutor.* **2007**, *9*, 18–48. [[CrossRef](#)]
31. Morelli, M.; Mengali, U. A Comparison of Pilot-Aided Channel Estimation Methods for OFDM Systems. *IEEE Trans. Signal Process.* **2001**, *49*, 3065–3073. [[CrossRef](#)]

Publisher’s Note: MDPI stays neutral with regard to jurisdictional claims in published maps and institutional affiliations.



© 2020 by the authors. Licensee MDPI, Basel, Switzerland. This article is an open access article distributed under the terms and conditions of the Creative Commons Attribution (CC BY) license (<http://creativecommons.org/licenses/by/4.0/>).